Long-Range Ordering of Oxygen-Vacancy Planes in α-Fe_2O_3 Nanowires and Nanobelts

Zhiqiang Chen,*,† Uroš Cvelbar,§ Miran Mozetič,§ Jiaqing He,|| and Mahendra K. Sunkara*,†,‡

Institute for Advanced Materials & Renewable Energy and Department of Chemical Engineering, University of Louisville, Louisville, Kentucky 40292, Plasma Laboratory F4, Jozef Stefan Institute, Jamova 39, Ljubljana SI-1000, Slovenia, and Center for Functional Nanomaterials, Brookhaven National Laboratory, Upton New York 11973

Received January 28, 2008. Revised Manuscript Received February 22, 2008

We observed two long-range-ordering structures of oxygen vacancies, one in every tenth plane of $(3\bar{3}0)$ and another in every fourth plane of $(1\bar{1}2)$ in α-Fe_2O_3 nanowires and nanobelts synthesized under the same conditions. Interestingly, both types of oxygen-vacancy structures found in different nanowires have an equivalent ordering distance of 1.45 or 1.47 nm and were parallel to the growth direction of the nanowires and nanobelts. Lattice mismatch induced strain at the growth temperatures seems to justify the observed vacancy-ordering distance and may explain the reason for occurrence of such oxygen-vacancy ordering in various metal oxide nanowires grown from using both foils and catalyst clusters.

Introduction

Nanotubes and nanowires of metal oxides,[1–3] such as hematite (α-Fe_2O_3) nanowires, have attracted tremendous interest due to their potential applications in catalysis,[4,5] semiconductor devices,[6] sensors,[7,8] magnetic storage media,[9] and instruments for clinical diagnosis and treatments.[10] The crystal structure of hematite α-Fe_2O_3 can be described as hexagonal unit cell, with hcp (hexagonal close packed) arrays of oxygen anions stacked along the [001] direction, wherein iron cations occupy two-thirds of the sites.[10] Stacking faults and twin boundary layers were found in the synthesized Fe_2O_3 nanowires.[11–13] Particularly, the oxygen vacancies were found ordered in the plane of $1/5(3\bar{3}0)$.[11] Later, this ordering was found to be $1/10(3\bar{3}0)$ in the annealed α-Fe_2O_3 nanowires.[12] More interestingly, the oxygen-vacancy ordering resulted in the p-type conductivity of α-Fe_2O_3,[13] indicating that the electronic and optical behavior of the oxygen-deficient metal oxide nanowires could be different depending upon the kind of oxygen-vacancy ordering observed. However, the origin of such ordering of oxygen-vacancy planes in nanowires still remains unclear.

Recently, a different process involving direct plasma oxidation of bulk materials has been successfully applied for the rapid synthesis of a high density of metal oxide nanowires.[14,15] Specifically, α-Fe_2O_3 nanowires and nanobelts were produced by rapid oxidation of iron foils using highly dissociated oxygen plasma. In this process, iron species are not supplied from the vapor phase. The nanowires primarily grow in a basal mode, which is different from the traditional methods utilizing tip-led growth of nanowires via catalytic clusters. As this growth methodology is very much different from traditional ones, we have extensively studied the oxygen-vacancy ordering in these iron oxide nanowires using high-resolution electron microscopy (HREM).

Experimental Section

Synthesis. The iron oxide nanowires and nanobelts were synthesized directly from the solid foils by plasma oxidation during the exposure of Fe to the oxygen plasma. A commercially available low-purity (98.85% mass) iron substrate 3 mm thick was treated with an rf glow plasma generated in oxygen at 100 Pa for 120 s, where the sample surface was heated to 600 °C. The detailed process is described elsewhere.[15]

Characterization. Synthesized nanowires or nanobelts were scratched from a sample's surface, and suspended in ethanol solution and dispersed on a 300-mesh copper grid with a thin layer

* Corresponding authors. E-mail: mahendra@louisville.edu (M.K.S.); zhiqiang.chen@monsanto.com (Z.C.).
† Institute for Advanced Materials & Renewable Energy, University of Louisville.
‡ Department of Chemical Engineering, University of Louisville.
§ Jozef Stefan Institute.
|| Brookhaven National Laboratory.

(1) Shankar, K. S.; Raychaudhuri, A. K. *Mater. Sci. Eng., C* **2005**, *25*, 738–751.
(2) Ostrikov, K.; Murphy, A. B. *J. Phys. D* **2007**, *40*, 2223–2241.
(3) Ostrikov, K. *Rev. Mod. Phys.* **2005**, *77*, 489–511.
(4) Ohmori, T.; Takahashi, H.; Mametsuka, H. *Phys. Chem. Chem. Phys.* **2000**, *2*, 3519–3522.
(5) Liu, S. Q.; Huang, K. L. *Sol. Energy Mater. Sol. Cells* **2005**, *85*, 125–131.
(6) Li, S. Y.; Lee, C. Y.; Lin, P. *J. Vac. Sci. Technol., B* **2006**, *24*, 147–151.
(7) Wan, Q.; Li, Q. H.; Chen, Y. J. *Appl. Phys. Lett.* **2004**, *84*, 3654–3656.
(8) Deb, B.; Desai, S.; Sumanasekera, G. U.; Sunkara, M. K. *Nanotechnology* **2007**, *18*, Art. No. 285501:1-7.
(9) Kim, C. H.; Chun, H. J.; Kim, D. S. *Appl. Phys. Lett.* **2006**, *89*, Art. No. 223103,1-3.
(10) Cornell, R. M.; Schwertmann, U. *The Iron Oxide: Structure, Properties, Reactions, Occurrence, and Uses*; VCH: New York, 1996..
(11) Chueh, Y. L.; Lai, M. W.; Liang, J. Q. *Adv. Funct. Mater.* **2006**, *16*, 2243–2251.
(12) Lee, Y. C.; Chueh, Y. L.; Hsieh, C. H. *Small* **2007**, *8*, 1356–1361.
(13) Fu, Y. Y.; Wang, R. M.; Xu, J. *Chem. Phys. Lett.* **2003**, *379*, 373–379.
(14) Mozetic, M.; Cvelbar, U.; Vaddiraju, S.; Sunkara, M. K. *Adv. Mater.* **2005**, *17*, 2138–2142.
(15) Cvelbar, U.; Chen, Z. Q.; Sunkara, M. K.; Mozetic, M. Submitted for publication in *Small*, **2008**.

10.1021/cm800288y CCC: $40.75
Published on Web 04/22/2008

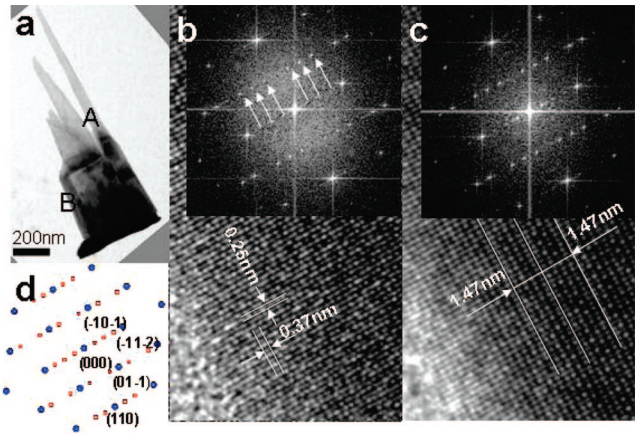

Figure 1. (a) ZLP filtered image showing straight α-Fe_2O_3 nanowires partly merged to form a nanobelt. (b) HREM image taken in region A; the inset FFT image shows extra maxima (indicated by arrows). (c) HREM image taken from region B presenting clear ordering features with a ordering distance of 1.47 nm; the inset FFT image shows that this ordering is the same as the one in region A. (d) Indexed schematic drawing of FFT image, where the ordering plane in α-Fe_2O_3 is 1/4(1$\bar{1}$2).

of carbon film for transmission electron microscopic (TEM) observations. The individual nanowires or nanobelts were separated while the TEM specimens were prepared. Conventional high-resolution electron microscopy (HREM) was performed using a field-emission TECNAI F20 XTWIN TEM equipped with Gatan GIF 2002 system operated at 200 kV. The superstructure models were constructed using Crystalkit software and the high-resolution image simulations were carried out using MacTempas software.

Results and Discussion

Figure 1a shows the typical structure of the synthesized iron oxide nanowire on one end of a palm-shaped nanobelt. Both nanowire and nanobelts have the same crystal structure. Both exhibit a new oxygen-vacancy superstructure in the (1$\bar{1}$2) plane with an ordering of 1/4(1$\bar{1}$2) found in α-Fe_2O_3 nanowires and nanobelts. The HREM image in Figure 1b taken at position A has lattice fringe distances of 0.37 and 0.25 nm that correspond, respectively, to the *d*-spacings of the α-Fe_2O_3 (1$\bar{1}$2$\bar{}$) and (110) planes, respectively. Visible bands are regularly present in the HREM images separated by a distance of 1.47 nm. Interestingly, extra maxima can be seen in the corresponding fast Fourier transform (FFT) image (inset in Figure 1b). The *d*-spacing of the maxima closest to the transmitted beam is about 1.47 nm, which is precisely 4 times the *d*-spacing of the (1$\bar{1}$2) plane. The extra maxima resemble the SAD pattern of α-Fe_2O_3 nanowire reported before.[11,12] However, these extra maxima originate from the oxygen vacancies that lie in a different plane compared to those previously reported.[11,12] A similar oxygen-vacancy-ordering structure is also found in the nanobelts. The HREM image (Figure 1c) taken from position B shows clear bands at a distance of 1.47 nm, and an extra maximum is present in its FFT image. We concluded that both the palm-shaped belt and the finger-shaped nanowire have the same structure in terms of an oxygen-vacancy ordering of 1/4(1$\bar{1}$2). The FFT images also show that both the nanowires and the

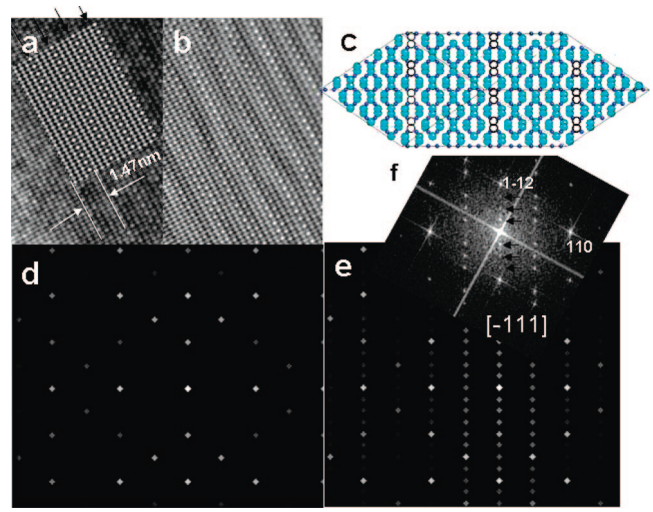

Figure 2. (a) Enlarged HREM image with simulated HREM image (inset) of the superstructure that matches the simulated image. (b) Reconstructed masked inverse FFT image showing a clear ordering band structure. (c) Superstructure constructed with induced 1/4(1$\bar{1}$2) oxygen vacancies in α-Fe_2O_3 structure. (d−f) FFT image (d) of the original HREM image taken from region B (Figure 1c) with the simulated diffraction pattern of the superstructural model (e) showing the extra maxima caused by oxygen-vacancy ordering, and a simulated diffraction pattern of stoichoimistric α-Fe_2O_3 with a thickness of 35 nm (f).

nanobelts have the same growth direction of [110]. In addition, the oxygen-vacancy planes (1$\bar{1}$2) are parallel to the growth direction in both forms.

To confirm the structure of this oxygen-vacancy ordering, we constructed a superstructural model, $a' = b' = 4a = 4b = 2.0136$ nm, and $c' = 4c = 5.4808$ nm (as shown in Figure 2c), with oxygen vacancies on every fourth (1$\bar{1}$2) plane. The corresponding high-resolution TEM image was simulated using MacTempas software. The simulated HREM image (inset of Figure 2a) was obtained using a defocus of 4 nm, a thickness of 35 nm, and the [$\bar{1}$11] zone axis; it matches well with the experimental image shown in Figure 2a. The arrows indicate the position of the oxygen-vacancy planes. The same image, shown in Figure 2b, was reconstructed using the obtained FFT mask. It is noticeable that the ordering feature coincides with the column of oxygen vacancies in the plane of (1$\bar{1}$2), wherein the oxygen vacancies formed in pairs and aggregate linearly. The diffraction pattern obtained from the FFT image (Figure 2f) also agrees well with the calculated diffraction pattern (DP) (Figure 2e) of the constructed superstructure model. This DP estimated in Figure 2d is assessed as stochiometric α-Fe_2O_3. As the DPs are calculated using same thickness for both the oxygen-vacancy superstructure and stoichiometric Fe_2O_3 models, we can see that the extra maxima in the DPs of superstructure model are originating from the oxygen-vacancy ordering, and not from the double diffraction (Figure 2d,e). This leads us to conclude that the oxygen-vacancy ordering is formed in the planes 1/4(1$\bar{1}$2) of α-Fe_2O_3 nanowires and nanobelts.

In addition to this ordering in the plane of α-Fe_2O_3(1$\bar{1}$2), another superstructure in the (3$\bar{3}$0) plane with an ordering of 1/10(3$\bar{3}$0) was observed. In the conventional HREM image (Figure 3b) from the larger nanowire region A (Figure 3a), blurred ordering bands are visible. The *d*-spacing of the extra

(16) Colliex, C.; Manoubi, T.; Ortiz, C. *Phys. Rev. B* **1991**, *44*, 11402–11411.

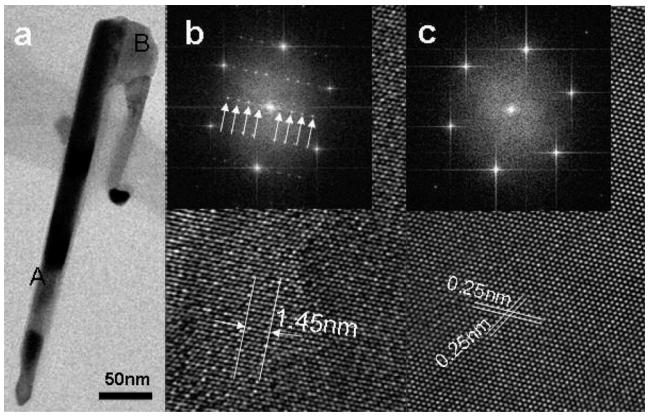

Figure 3. (a) BF TEM image with analysis spots (marked) showing the straight α-Fe_2O_3 nanowire with a tip and merger area with nanowire of different orientation. (b) HREM image taken from the A region showing an ordering distance of about 1.45 nm, and the corresponding fast Fourier transform (FFT) image on the bottom illustrating that ordering occurred by 1/10(3$\bar{3}$0). (c) HREM image taken from position B revealing few ordering features.

maxima in FFT image (Figure 3b) closest to the transmitted beam is about 1.45 nm, which is 10 times the *d*-spacing in the (3$\bar{3}$0) plane. The vacancy-ordering distance in our present observation was further confirmed to be the same as that in ref 12, instead of 5 times the *d*-spacing of plane (3$\bar{3}$0) as reported earlier (ref 11). This value of the distance seems to be the equivalent of the above ordering distance of 1/4(1$\bar{1}$2) considering possible lattice distortion. Our further analyses also confirmed the presence of an oxygen-vacancy ordering of 1/10(3$\bar{3}$0) in the α-Fe_2O_3 nanobelts. This finding indicates that the formation of nanowires or nanobelts is independent of the oxygen-vacancy ordering.

Similarly, we constructed a superstructure model with oxygen vacancies in every 10 (3$\bar{3}$0) planes (Figure 4) with the following lattice parameters: $a' = b' = 10a = 10b =$ 5.034 nm and $c' = c = 1.375$ nm. The corresponding high-resolution TEM images were simulated using a defocus of −39 nm and a thickness of 25 nm. The simulated HREM image (Figure 4a), obtained with the [001] zone axis, matches well with the experimental image (Figure 4c). The white circles in Figure 4b indicate the positions of oxygen vacancies. This ordering feature, seen in the image as the blurred bands, coincides with the column of oxygen vacancies in the plane of (3$\bar{3}$0). After comparing the integrated diffraction patterns of the model (Figure 4h) with those of the stoichiometric α-Fe_2O_3 (Figure 4g), we concluded that the extra maxima in the DPs of the superstructure model originate from the oxygen-vacancy ordering in the planes of 1/10(3$\bar{3}$0).

The formation of oxygen-vacancy ordering still is unclear, though it has been reported for many oxides, particularly in ferromagnetic and superconducting perovskite oxides.[17–21]

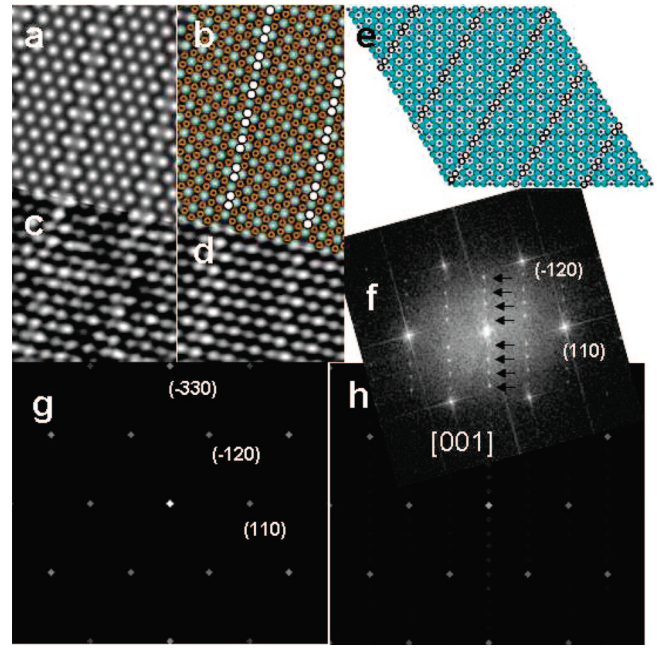

Figure 4. (a) Simulated HRM image with overlaying atoms drawn in. (b) HREM image showing that the blurred bands in the image correspond to the positions of the oxygen-vacancy planes. (c) Matching of the simulated image with that of the HREM image taken from region A (Figure 1c). (d) Reconstructed inverse FFT image with a mask on the maxima showing clear ordering features. (e) Superstructure model constructed with dimensions $a' = 10a_{\alpha\text{-}Fe_2O_3}$, $b' = 10b_{\alpha\text{-}Fe_2O_3}$, and $c' = c_{\alpha\text{-}Fe_2O_3}$, and with oxygen-vacancy ordering at 1/10(3$\bar{3}$0). (f) FFT of the HREM image taken from region A (Figure 1c) with the simulated diffraction pattern of stoichiometric α-Fe_2O_3 with a thickness of 25 nm. (g) Simulated diffraction pattern of the superstructural model. (h) Illustration of the extra maxima caused by oxygen-vacancy ordering.

In the latter, the long-range ordering of oxygen vacancies generally was thought to reflect the replacement of a high and low cationic oxidation state, i.e., Ti^{4+} with Fe^{3+}. In such cases, one or more oxygen atoms must be removed to retain the neutral charge balance. Nevertheless, this mechanism cannot apply to the present observations in pure binary oxide systems.

A study of $Nb_{12}O_{29}$ revealed that the formation of oxygen-vacancy pairs at the nearest-neighbor sites is energetically favorable.[22] Our observations with α-Fe_2O_3 (shown in Figures 2c and 4e) also suggest that the oxygen vacancies form in pairs. A relaxation displacement model, similar to that used for sodium vacancy in a NaCl crystal,[23] was used for α-Fe_2O_3 by considering only the nearest-neighbor interactions. The arrows in Figure 5a show the directions of stresses generated using a single oxygen vacancy; evidently, this resulted in a tendency for both the oxygen and iron ions to move. However, a pair of oxygen vacancies led to a more stable structure with balanced stresses (Figure 5b). Moreover, once a single oxygen vacancy forms, less energy is needed to form a second vacancy next to the first one, since the valence strength of the O−Va−Fe that is generated is weaker than that of O−Fe. After a pair of oxygen vacancies has formed, the second pair could be parallel to the first pair, or

(17) Klenov, D. O.; Donner, W.; Forran, B. *Appl. Phys. Lett.* **2003**, *82*, 3427–3429.
(18) Iijima, S. *Acta Crystallogr.* **1975**, *A31*, 784–790.
(19) Travlos, A.; Boukos, N.; Apostolopoulos, G. *Appl. Phys. Lett.* **2003**, *82*, 4053–4055.
(20) Rohrbach, A.; Hafner, J.; Kresse, G. *Phys. Rev. B* **2004**, *70*, Art. No. 12542, 1-16.
(21) Chaillout, C.; Alario-Franco, M. A.; Cappononi, J. J. *Phys. Rev. B* **1987**, *36*, 7118–7120.
(22) McCammon, C. A.; Becero, A. I.; Langenhorst, F. *J. Phys.: Condens. Matter* **2000**, *12*, 2969–2984.
(23) Kelly, A.; Groves, G. W. *Crystallography and Crystal Defects*; Addison Wesley Publishing Company: Reading, MA, Menlo Park, CA, 1970; p 269.

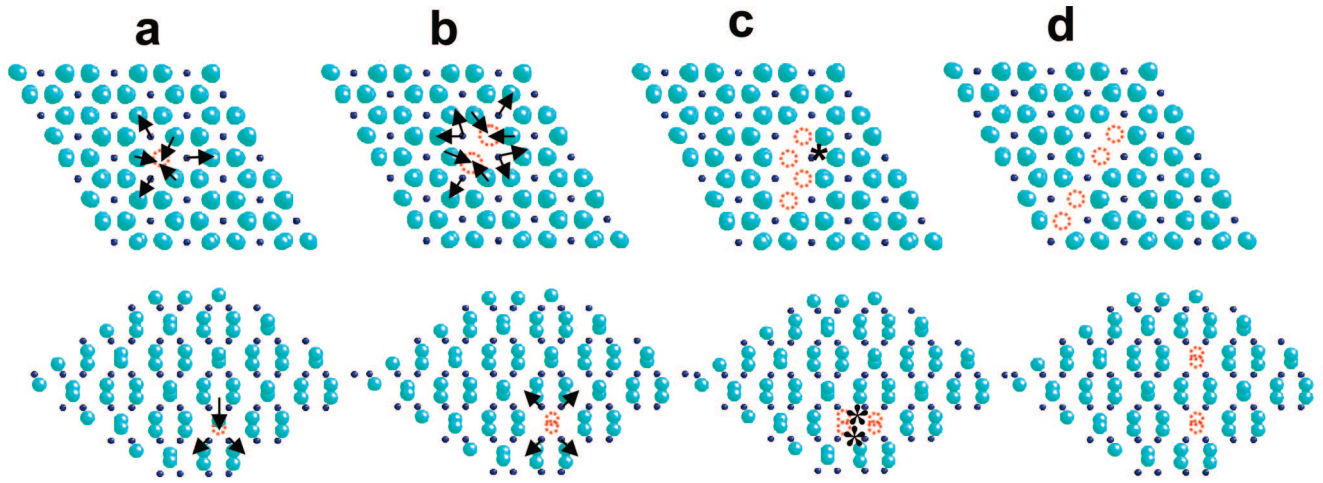

Figure 5. (a) Schematic drawing of a single oxygen vacancy showing that it is not a stable structure and indicating the formation of O−Va−Fe valence. (b) Schematic drawing of a pair of vacancies in the $(3\bar{3}0)$ (top) and $(1\bar{1}2)$ (bottom) planes of α-Fe_2O_3 wherein a balanced local stress leads to a stable structure. (c) Schematic drawing of parallel oxygen-vacancy pairs depicting a balanced local stress, but a much lower oxidization state of (∗) iron atom. (d) Schematic drawing of linear oxygen-vacancy pair chain in the $(3\bar{3}0)$ (top) and $(1\bar{1}2)$ (bottom) planes of α-Fe_2O_3 that resulted in a balanced local stress as well as a higher oxidization state of (∗) iron atoms. (O ion, sky blue; Fe ion, blue; Va, red dashed circle).

aligned with it to form a chain of oxygen vacancies. If the pairs were parallel, then one of the iron ions next to the vacancies would have a much lower oxidization state with high internal energy and, hence, would not be energetically favorable (Figure 5c). When pairs of oxygen vacancies form in a chain, all of the iron and oxygen ions next to the oxygen vacancies have the same state, presumably considered as lower internal energy (Figure 5d).

The above discussion might explain how the oxygen vacancies assume a linear dimension during the growth of an iron oxide nanowire. However, why do two oxygen-vacancy orderings occur in the α-Fe_2O_3 nanowires/nanobelts, and why are they properly situated on the planes of $(3\bar{3}0)$ or $(1\bar{1}2)$ with the same large ordering distance? In the present study, our nanowire/nanobelts are directly grown from the iron alloy bulk and the growth direction was [110]. The nucleation of α-Fe_2O_3 is likely to follow a certain orientation relationship to the iron substrate, and thus, α-Fe_2O_3 may have grown in an epitaxial relationship with its iron-foil substrate. Although there is little evidence of a direct orientational relationship between α-Fe_2O_3 and iron substrate, this relation can be derived from the relationship between Fe and FeO, FeO and Fe_3O_4, and Fe_3O_4 and Fe_2O_3. The formation of FeO from iron followed the orientation relationships of $(001)_{Fe}//(001)_{FeO}$ and $[100]_{Fe}//[110]_{FeO}$.[24] There also are such relationships between FeO and Fe_3O_4: $(001)_{FeO}//(001)_{Fe_3O_4}$ and $[110]_{FeO}//[100]_{Fe_3O_4}$. Then the orientation relationships between Fe_3O_4 and Fe would be $(001)_{Fe}//(001)_{Fe_3O_4}$ and $[100]_{Fe}//[100]_{Fe_3O_4}$. Then again the orientation relationship between α-Fe_2O_3 and Fe_3O_4 is known to be $(111)_{Fe_3O_4}//(0001)_{Fe_2O_3}$ and $[1\bar{1}0]_{Fe_3O_4}//[10\bar{1}0]_{Fe_2O_3}$.[25] Therefore, the direct orientational relationship between α-Fe_2O_3 and iron substrate could be derived from $(111)_{Fe}//(0001)_{Fe_2O_3}$ and $[1\bar{1}0]_{Fe}//[10\bar{1}0]_{Fe_2O_3}$. The ordering planes $1/2(3\bar{3}0)_{Fe_2O_3}$ and $(1\bar{1}2)_{\alpha\text{-}Fe_2O_3}$ are, respectively, parallel to $(12\bar{3})_{Fe}$ and $(001)_{\alpha\text{-}Fe}$. The mismatch between these two planes can be calculated with the equation $\delta_s = (d_f - d_s)/d_s$, where d_f and d_s are the *d*-spacings of α-Fe_2O_3 and the iron substrate planes. Indeed, our calculated mismatch between $1/2(3\bar{3}0)_{Fe_2O_3}$ and $(12\bar{3})_{Fe}$, $(1\bar{1}2)_{\alpha\text{-}Fe_2O_3}$ and $(001)_{\alpha\text{-}Fe}$, are, correspondingly, about 5.2% and ∼27.9% at 600 °C. The lattice parameters of α-Fe_2O_3 and Fe at 600 °C were taken from ref 26, so that mismatch caused by thermal stress is already included. If we assume that the oxygen-vacancy planes of $(3\bar{3}0)$ and $(1\bar{1}2)$ are an array of edge dislocations, the Burgers vector would be $\mathbf{b} = 1/2[3\bar{3}0]$, $[1\bar{1}2]$, respectively. The relaxation distance of this edge dislocation is given by $d_{RD} = |b|/\delta_s$.

The calculated dislocation relaxation distances are then 1.405 and 1.329 nm for $(3\bar{3}0)$ and $(1\bar{1}2)$, respectively. However, there still are differences of ∼3.8% and ∼10% between our experimental observations and the calculated distances. However, we note that the calculated distances did not include the possibility of deformation of the iron substrate. At 600 °C, the *d*-spacing of α-$Fe_2O_3(1\bar{1}2)$ is about 0.371 nm, while that of Fe(001) is about 0.29 nm. This difference in lattice spacings would impose a compressed stress on α-$Fe_2O_3(1\bar{1}2)$ and a tensile stress on Fe(001). Hence, the deformation of Fe(001) would be much easier than that of α-$Fe_2O_3(1\bar{1}2)$. Therefore, it is reasonable to attribute the formation of the oxygen-vacancy planes to the relaxation of interfacial stress between α-Fe_2O_3 and the iron substrate and, similarly, very likely that the oxygen-vacancy orderings originate from the expitaxial growth of α-Fe_2O_3 nanowires/nanobelts. Indeed, other researchers working on STO found that interfacial and thermal stress caused the growth of oxygen-vacancy-ordered planes parallel or perpendicular to the interface of the epitaxially grown thin film.[17] However, there are a few reports of oxygen-vacancy ordering in different planes of oxides. The above model also may explain the formation of oxygen-vacancy-plane ordering in metal oxide nanowires grown via the tip-led growth mode. Even in these cases the interfacial stresses at the synthesis

(24) Corkovic, S.; Pyzalla, A. R. *Mater. Corros.* **2004**, *55*, 341–351.
(25) Watanabe, Y.; Ishii, K. *Phys. Status Solidi A* **1995**, *150a*, 673–686.
(26) Gorton, A. T.; Bitsianes, G.; Joseph, T. L. *Trans. AIME* **1965**, *233*, 1519–1525.

temperature could trigger the formation of oxygen-vacancy planes in an ordered fashion.

It is very likely that all oxides might have more than one oxygen-vacancy-ordering plane. Indeed, our recent investigations of tungsten oxide nanowires demonstrated that at least two oxygen-vacancy planes were present. Similar results were obtained with Nb_2O_5 nanowires. These results on Nb_2O_5 and WO_3 nanowire systems will be detailed later.

Conclusions

In summary, we studied long-range ordering of iron oxide nanostructure planes derived by a new direct plasma synthesis. We found that there are two oxygen-vacancy-ordered superstructures from different planes in α-Fe_2O_3 nanowires, which have an equivalent ordering distance. These two long-range-ordering superstructures were explained by the introduction of oxygen vacancies in the planes of $1/10(3\bar{3}0)$ and $1/4(1\bar{1}2)$ in the α-Fe_2O_3 nanowires/nanobelts. Both oxygen-vacancy planes share similar ordering distances of 1.45 and 1.47 nm, and lie parallel to the growth direction of the nanowires. The formation of such ordering was attributed to the relaxation of a stress at the interface between α-Fe_2O_3 and its iron substrate during the growth of nanowires/nanobelts.

Acknowledgment. The authors acknowledge support from the U.S. Department of Energy for the Institute for Advanced Materials & Renewable Energy at the University of Louisville (DE-FG02-05ER64071), support from U.S. Department of Energy EPSCOR program (DE-FG36-05G085013 A), and the support from the Slovenian Ministry for Science and Technology (BI-SLO-ZDA-2006/07-01).

CM800288Y